# STUDY OF CRACK GROWTH IN MULTILAYERED CERAMIC/CERAMIC MATERIALS WITH STRONG INTERFACES

M. Kotoul [1]*, O. Sevecek [1], T. Vyslouzil [2] , R. Bermejo[3]

[1]*Institute of Solid Mechanics, Mechatronics and Biomechanics, Faculty of Mechanical Engineering, Brno University of Technology, Technická 2, 616 69, Brno, Czech Republic*
[2]*Jan E. Purkyne University, Na okraji 1001, 400 96 Usti nad Labem, Czech Republic*
[3]*Montanuniversität Leoben , Institut für Struktur- und Funtionkeramik, Peter-Tunner Straße 5, 8700 Leoben, Austria*
**kotoul@fme.vutbr.cz*

**Keywords:** layered ceramics, strong interfaces, Finite fracture mechanics.

**Abstract**
*FE modelling of a cracked four points bending specimen is carried out assuming that the specimen was fabricated from ATZ/AMZ ceramic laminate. The multilayer consists of nine alternating layers of different thickness, while the total thickness of the laminate body is kept constant. All the layers made of the same material, ATZ (alumina with 5% tetragonal zirconia), or AMZ (alumina with 30% monoclinic zirconia), respectively have the same thickness. Matched asymptotic procedure is used to derive the change of potential energy due to the perturbation caused by a branched crack extension of the total length $a_p$ or a straight penetrating crack extension of length $a_p$. Numerical simulations are compared with experimental observations.*

## 1 Introduction

It is now well recognized that a design of layered ceramic composites provides a promising way for to enhance the strength reliability of ceramic component as well as to improve their fracture toughness by e.g. crack deflection or crack bifurcation. Moreover, expansion coefficients between different layers inevitably generate thermal residual stresses during subsequent cooling of layered ceramics with *strong interfaces*. Compressive residual stresses significantly contribute to toughening effect and resulting R-curve behaviour. The elastic mismatch of the layers induces an additional crack driving force term. The propagation of a crack in a direction orthogonal to the laminate planes can be promoted (anti-shielding) or retarded (shielding) by the different elastic properties.

The apparent R-curve behaviour is usually studied assuming straight crack propagation perpendicularly across layer interfaces. Nevertheless, the propagation of the crack through the layers may occur with an angle different from straight propagation [1],[2].The compressive stress ensures that crack growth leading to failure in the laminar system is mediated by threshold strength, but, in some cases, it also leads to bifurcation of the propagating crack. Unfortunately, none of the theories regarding the directional growth of a crack in a brittle material such as deviation to maximize the crack tip energy release rate, deviation from the

established path when there is a positive T-stress, and cracks that choose the path that gives a zero value of the Mode II stress intensity factor is in agreement with the observed behaviour in the layered composites. For that reasons the problem is revisited using the concept of Finite fracture mechanics (FFM) [3]. The criterion used in this method can be stated as follows: failure will occur if there is sufficient energy available to allow a finite amount of crack growth denoted as $a_p$. The value of $a_p$ is assumed to be a material constant.

## 2 Experimental

The mechanical behaviour of a layered ceramic composed of thin layers of $Al_2O_3$ with 30% monoclinic $ZrO_2$ (referred to as AMZ layers), sandwiched between thicker layers of $Al_2O_3$ with 5% tetragonal $ZrO_2$ (ATZ layers) was tested under the four–point bending. The volume ratio between the AMZ and ATZ material, i.e. $V_{AMZ}/V_{ATZ}$, was ca. 1/6. The properties of both materials were determined in monolithic samples [4] and are listed in Table 1.

| Material | $E$ [GPa] | $\nu$ [-] | $\alpha$ x$10^6$ [$K^{-1}$] | $\sigma_f$ [MPa] | $K_{Ic}$ [MPa.$m^{1/2}$] | $G_c$ [J/$m^2$] |
|---|---|---|---|---|---|---|
| ATZ | 390±10 | 0.22 | 9.8±0.2 | 422±30 | 3.2±0.1 | 25±2 |
| AMZ | 280±10 | 0.22 | 8±0.2 | 90±20 | 2.6±0.1 | 23±2 |

**Table 1**. Material properties of the laminate components

In order to investigate the crack propagation in the laminate, a sharp notch of depth 300μm and tip radius of ca. 25 μm, was introduced in the first ATZ layer following the standard SEVNB procedure according to ISO 23146. Due to the tensile residual stresses in the first layer a local stress intensity factor at the crack tip overcomes the fracture toughness $K_{Ic}$ of the ATZ layer during the notching process. Thus, a crack between the notch and the first ATZ/AMZ interface originated without any additional mechanical load (see close-up in Fig. 1a). This was the initial state of the specimen (i.e. crack terminating at the first interface).

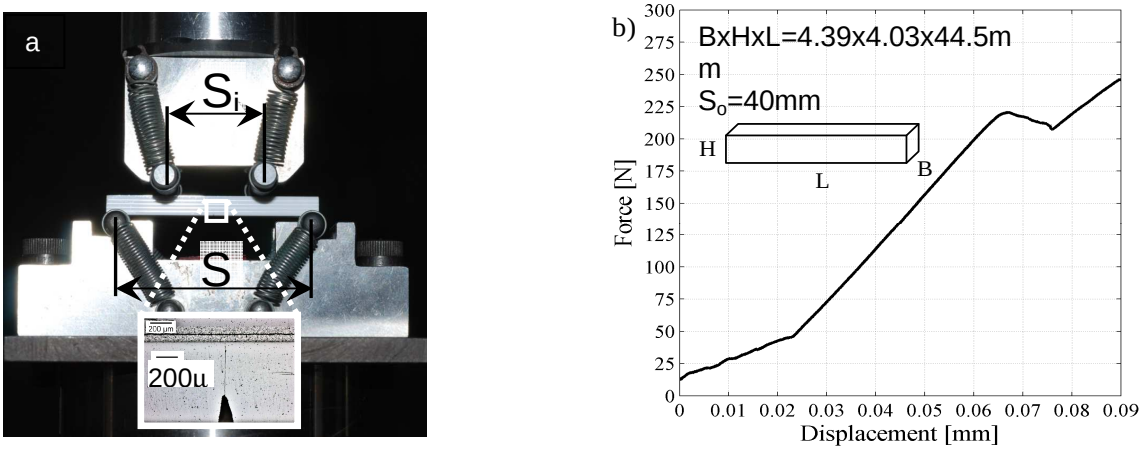


**Figure 1**. a) Test configuration of the four-point bend experiment on a notched specimen and b) load-displacement curve recorded during testing.

To assess the crack propagation through the laminate, the notched specimen was loaded in four–point bending (inner and outer spans: 20 mm and 40 mm respectively) at a constant displacement rate of 0.5 mm/min using a universal testing machine (Zwick Z010, Switzerland). The testing jig is represented in Fig. 1a. The corresponding load–displacement curve is shown in Fig. 1b. The first region of the curve (up to 40 N) is associated with the alignment of the rollers during the test. Above 50 N up to 215 N a linear behaviour can be observed: the crack is arrested at the interface until the critical loading force reaches

approximately 220 N. Then a decrease in load can be appreciated, which corresponds to the propagation of the crack through the compressive layer. At this point a sudden crack bifurcation occurs and propagation of both cracks branches proceeds towards the next interface. The propagation angle of the bifurcated crack is shown in Fig.2.

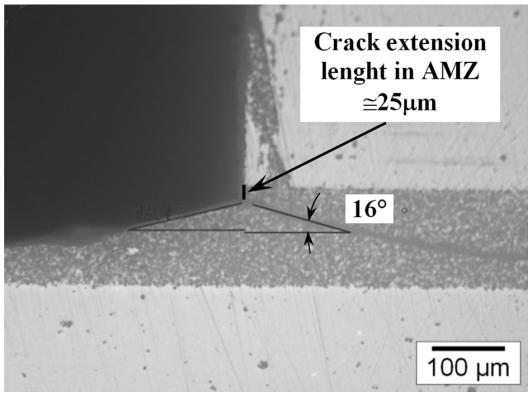


**Figure 2.** Crack path in the compressive layer of specimen #1. Picture taken after polishing ca. 250μm from the lateral face of the laminate. Volume ratio of the materials is $V_{AMZ}$ / $V_{ATZ}$ = 1/6.

## 3 Theoretical model of crack propagation in ceramic laminates

2D FEM model of a laminate was created, see Fig. 3. In contrast with the experiment, no notch was modelled – only a straight crack which is a sufficient simplification of the problem. The total model height is 4.03 mm and it corresponds to the real specimen height. The width of the 2D model was considered as unit together with element plane strain condition. The applied loading force *F* in FEM calculations is then always related to this unit width, i.e. in comparison with the experimental data in Fig.1b, is multiplied by factor 1/*B*. In the first part of the computational analysis, the apparent R-curve of a laminate with a given residual

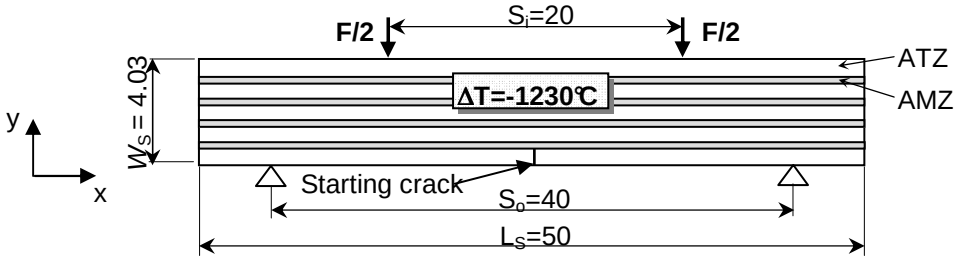


**Figure 3**. Scheme of a laminate used for the calculations.

stress profile was calculated assuming a straight crack propagation. The equilibrium condition at the crack tip was considered, i.e. crack propagation is possible if the stress intensity at the crack tip, $K_{Itip}$ for the crack length *a* equals or exceeds the intrinsic material toughness $K_{Ic}$.

$$K_{Itip}(a) = K_{Ic},\ K_{Itip}(a) = K_{Iappl}(a) + K_{Ires}(a). \tag{1}$$

Thus, solving Eq .(1) for $K_{appl}(a)$, the crack propagation criterion is fulfilled when

$$K_{Iappl}(a) = K_{Ic} - K_{Ires}(a) = K_{IR}(a), \tag{2}$$

where $K_{Iappl}$ is the applied stress intensity, $K_{Ires}$ is the stress intensity contribution from the residual stresses and $K_{IR}(a)$ can be understood as the apparent toughness. The displacement-

matching approach was used to the calculation of the stress intensity factor. The results were obtained with quadrilateral elements collapsed to triangular quarter-point elements. All the layers made of the same material (ATZ or AMZ, respectively) have the same thickness, so the laminate is well defined by the thicknesses $t_{ATZ}$ and $t_{AMZ}$, or the specimen height $W_S$ and the volume ratio $\lambda = t_{AMZ}/t_{ATZ}$. It is apparent from the Table 1 that the AMZ layers are under compression since their thermal expansion coefficient is minor than that of the ATZ layers which are under tension. The crack face displacement data corresponding to the residual stresses were used for the calculation of the shielding stress intensity factor $K_{Ires}$. The apparent fracture toughness $K_{IR}(a) \leq K_{Iappl}$ was found by summation of the intrinsic material toughness $K_{Ic}$ and the shielding stress intensity factor $K_{Ires}$. Critical value of the loading force was obtained by dividing the value of the applied stress intensity factor $K_{Iappl}$ from Eq. (2) and the value of the stress intensity factor induced by unit force.

In the second part of the analysis the crack transition across an interface followed by crack bifurcation or deflection was modelled. An analytical description of the stress field in the vicinity of the crack tip terminating at the interface of two dissimilar materials is essential. Stress field description comprises a calculation of the singularity exponent, determination of the stress and displacement field distribution in the tip vicinity and calculation of the Generalized Stress Intensity Factors (GSIF) as well as the T-stress [6]. For the calculations of the Stress Intensity Factors, the two state integral method based on Betti´s reciprocal theorem was employed [6].

The singular stress field and displacement field for general stress concentrator are given by the first two terms of the asymptotic expansion:

$$\begin{aligned} \sigma_{ij} &= H_1 \cdot r^{\delta_1 - 1} \cdot f_{ij1}(\theta) + H_2 \cdot r^{\delta_2 - 1} \cdot f_{ij2}(\theta), \\ \mathbf{U}^0 &= H_1 \cdot r^{\delta_1} . \mathbf{u}_1(\theta) + H_2 \cdot r^{\delta_2} . \mathbf{u}_2(\theta), \end{aligned} \tag{3}$$

where $H_1$ and $H_2$ are generalized stress intensity factors (GSIF) and $\delta_1$, $\delta_2$ are the corresponding singularity exponents ($\delta_1 < \delta_2$) – see [5]. The functions $f_{ij}$ and $\mathbf{u}_i$, together with the mentioned singularity exponents, are calculated using a method based on the complex potentials. In some particular cases, $H_1$ is negligible and makes no contribution (e.g. case of a crack perpendicular to the interface under pure mode I of loading). Since the Energy Release Rate (ERR) for the crack terminating at the interface of two different materials is, for infinitesimally small crack increment, zero or infinite (depending on the singularity type), the classical Griffith approach cannot be applied. To bypass this problem, a theory of Finite Fracture Mechanics (FFM) was applied [3]. Infinitesimal crack increment was replaced by a finite increment and for this increment a change of the potential energy was calculated. The small perturbation parameter $\varepsilon$ is defined as $\varepsilon = a_p/W_S << 1$, where $W_S$ is the characteristic size of the specimen (e.g. specimen height). A second scale to the problem can be introduced, represented by the scaled-up coordinates $(y_1, y_2) = (x_1 / \varepsilon, x_2 / \varepsilon)$, which provides a zoomed-in view into the region surrounding the crack, see Fig. 4. The $x_i$ are coordinates at the crack tip but in the non-zoomed state, i.e. in case of the real specimen with adjacent interfaces [7]. In the zoomed coordinates, $y_i$, the influence of the adjacent laminate interfaces is not considered. In order to predict the mode of the further crack propagation (single or double crack penetration) and further propagation direction, the change of the potential energy $\delta\Pi_{a_p}$ or more precisely the so-called additional energy $\Delta W$, released by the fracture process has to be calculated, as given by [8]:

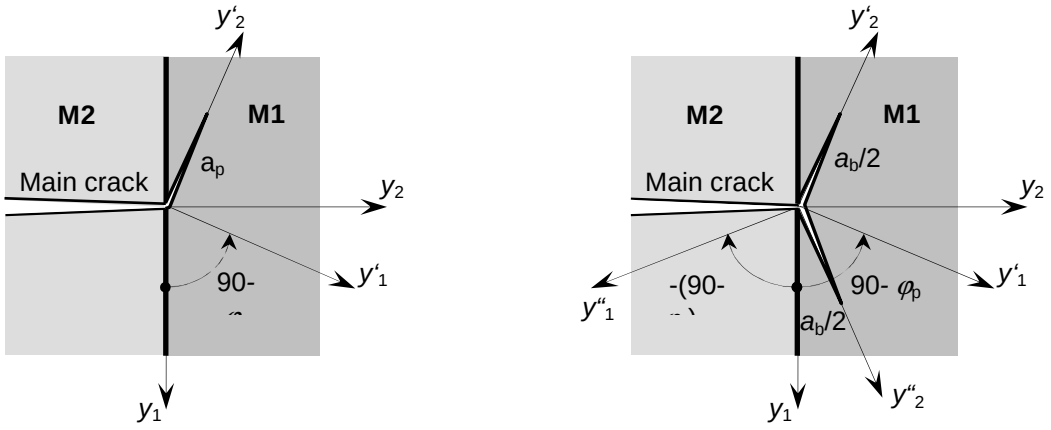


**Figure 4**. Scheme of a) single crack deflection and b) crack bifurcation (branching) at the interface between materials M2 and M1. A local Coordinate System is defined in the inner domain, where the crack extension length is given as $a_p = a_b/2 + a_b/2$.

$$\Delta W = \delta\Pi_{a_p} - G_c^{(M1)} a_p. \tag{4}$$

$G_c^{(M1)}$ is the critical energy release rate of material M1, which may be determined experimentally (see Table 1). The term $\delta\Pi_{a_p}$ expresses the change in the potential energy corresponding to a certain initial crack length increment, $a_p$. Calculation of $\Delta W$ was performed for several crack increment lengths in all possible crack propagation directions. Then a direction (and type of propagation) was chosen such that the additional energy $\Delta W$ reached a maximal value. The change of the potential energy $\delta\Pi_{a_p}$ considering both the thermal and flexural sources of the stress was calculated by integration of the energy release rate along the crack increment as given by:

$$\delta\Pi_{a_p} = \int_0^{a_{p0}} G\, da_{p(b)} = W_S \int_0^{\varepsilon_0} \left(G^{(1)} + G^{(2)} + \ldots\right) d\varepsilon, \quad \frac{G^{(2)}}{G^{(1)}} \to 0 \text{ for } \varepsilon \to 0 \text{ and } \delta_2 < 1 \tag{5}$$

where $W_S$ is the laminate height and $G$ is the energy release rate. It is worth mentioning that there are two sources of stress, i.e. mechanical ($m$) and residual ($r$) which, separately applied, give the crack extension forces $G_m$ and $G_r$. Under combined loading (flexural and thermal) the first term of the total crack extension force is given by:

$$\begin{aligned} G^{(1)} = {} & W_S^{2\delta_1} \frac{2\delta_1}{2W_S} H_1^{\,2} K_{1p(b)}\left(\varphi_p\right) \varepsilon^{2\delta_1 - 1} + W_S^{\delta_1+\delta_2} \frac{\delta_1+\delta_2}{2W_S} H_1 H_2 \varepsilon^{\delta_1+d_2-1} \cdot \\ & \cdot \left(K'_{1p(b)}\left(\varphi_p\right) + K_{2p(b)}\left(\varphi_p\right) \cdot \Psi_2\right) + W_S^{2\delta_2} \frac{2\delta_2}{2W_S} H_2^{\,2} K'_{2p(b)}\left(\varphi_p\right) \varepsilon^{2\delta_2 - 1} \geq 0 \end{aligned} \tag{6}$$

The second term of the crack extension force due to the combined loading is for the case of the crack bifurcation given by

$$
\begin{aligned}
G^{(2)} = {} & W_S^{1+\delta_1}\frac{\delta_1+1}{W_S}H_1\sigma_{res}^{(M1)}\varepsilon^{\delta_1}\cos^2\varphi_p\left(\int_0^{1/2}\mathcal{V}_{1y_1'}(y')\,dy_2' + \int_0^{1/2}\mathcal{V}_{1y_1''}(y'')\,dy_2''\right) - \\
& - W_S^{1+\delta_1}\frac{\delta_1+1}{W_S}H_1\sigma_{res}^{(M1)}\varepsilon^{\delta_1}\sin\varphi_p\cos\varphi_p\left(\int_0^{1/2}\mathcal{V}_{1y_2'}(y')\,dy_2' - \int_0^{1/2}\mathcal{V}_{1y_2''}(y'')\,dy_2''\right) + \\
& + W_S^{1+\delta_2}\frac{\delta_2+1}{W_S}H_2\sigma_{res}^{(M1)}\varepsilon^{\delta_2}\cos^2\varphi_p\left(\int_0^{1/2}\mathcal{V}_{2y_1'}(y')\,dy_2' + \int_0^{1/2}\mathcal{V}_{2y_1''}(y'')\,dy_2''\right) - \\
& - W_S^{1+\delta_2}\frac{\delta_2+1}{W_S}H_2\sigma_{res}^{(M1)}\varepsilon^{\delta_2}\sin\varphi_p\cos\varphi_p\left(\int_0^{1/2}\mathcal{V}_{2y_2'}(y')\,dy_2' - \int_0^{1/2}\mathcal{V}_{2y_2''}(y'')\,dy_2''\right) \gtrless 0,
\end{aligned}
\tag{7}
$$

where $\sigma_{res}^{(M1)}$ stands for residual stress. For the case of the single crack deflection, $G^{(2)}$ adopts the same form as Eq. (7), where only one integral (from 0 to 1 - for one branch) is considered within the parentheses. Note that GSIF or the T-stress is generally the sum of two contributions:

$$H_1 = H_1^m + H_1^r; \quad H_2 = H_2^m + H_2^r; \quad T = T^m + T^r, \tag{8}$$

where $H_i^m$ is due to pure flexural loading and $H_i^r$ is due to pure thermal loading respectively. These parameters characterize the stress state in the crack tip vicinity. Eqs. (6) and (7) simplify significantly when some of the GSIF ($H_1$ or $H_2$) is zero (e.g. the case of the crack perpendicular to the interface). The factors $K_{i\,p(b)}(\varphi_p)$ and the opening of the crack extension $\mathcal{V}_{2y_1'}(y')$, $\mathcal{V}_{2y_2'}(y')$, etc., are calculated by means of FEM on the inner domain once for all, since they depend only on the local geometry and material properties – for details see [5],[7].

## 4 Results

The calculated apparent fracture toughness is plotted in Fig. 5, as a function of the crack length *a*. For comparison, results obtained using the classical weight function concept originally developed for homogeneous samples are included. In this concept, the stress intensity factor is calculated considering an inhomogeneous distribution of the residual stresses in a homogeneous body with the elastic modulus of the first layer. Observe that the elastic mismatch of the layers is not taken into account by the weight function method. As already observed in previous works, the apparent toughness increases in the layers with compressive stress with increasing crack length, and it decreases in the layers with tensile stress as the crack continues to grow. $K_{IR}$ reaches its maximum or minimum values as the crack approaches the interface with a next layer of an opposite stress sign. The R-curve has to be considered as an effective (or apparent) property: for certain crack lengths the intrinsic positive toughness of the material is overcome by the effect of the tensile residual stresses. This means that cracks with this length will propagate spontaneously without addition of any external load. For example, the crack reaching the AMZ layer is initially influenced by the tensile residual stress in the fractured ATZ layer, hence $K_{IR}$ is lower than the intrinsic toughness of the material. As the crack grows, $K_{IR}$ increases above the intrinsic toughness due to the growing influence of the compressive residual stresses in the AMZ layer. Nevertheless, calculations revealed that the corresponding loading force needed for crack to grow in AMZ layer is systematically higher than the loading force recorded experimentally, see Fig. 1b. The cause of this behaviour is that the straight crack propagation is not a favoured mode of fracture and, instead, crack deflects or bifurcates in the compressive AMZ layer.

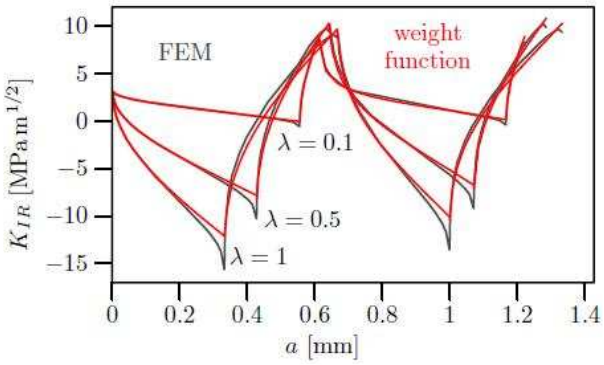


**Figure 5.** Apparent toughness as a function of crack length $a$ for several volume ratios λ

The crack path was predicted using the model described in the previous section. A competition between single crack penetration and crack bifurcation in case of the laminate defined in the previous section was investigated. Using Eqs. (5), (6) and (7) the change of the potential energy for several possible propagation directions was calculated and is represented in Fig. 6. Both, length of the crack extension $a_p$ and GSIF $H_2^m$ were varied in a wide range of values. The crack extension $a_p$ was varied in order to be always smaller than the radius of the domain where the singular stress field (3) prevails.

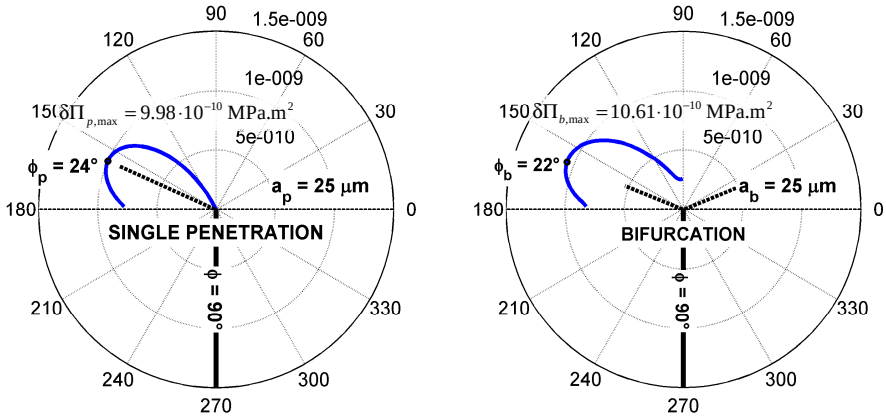


Figure 6. Variation of the change of the potential energy δΠ with the angle of the crack extension for a) single crack deflection and b) crack bifurcation. Crack extension length $a_p$=25μm, $H_2^r$=0.39 MPa.m$^{1-\delta 2}$ and $H_2^m$=1.1 MPa.m$^{1-\delta 2}$ (flexure load 220N).

The obtained numerical results showed that both crack bifurcation or crack deflection are preferred modes of fracture with respect to straight crack propagation. The angle of deflection/bifurcation, $\varphi_p$, was predicted to be in the range $20° - 30°$ which is in a good agreement with experimental observations. However, contrary to experimental data, the crack propagation was predicted even for the loading force about of 10 N, i.e. much lower value then the threshold value of 220 N found experimentally, see Fig.1b. This discrepancy made us re-examine the real crack path. By inspection of the fractographic observations in Fig. 2 it could be concluded that crack does not bifurcate and/or deflect just at the interface but at a distance $\Delta a \cong 25$ μm behind the interface. This is due to the energy accumulated in the system during the unstable crack propagation (i.e. in the ATZ layer which is subjected to tensile residual stress) before the crack reaches the interface. The stress field around the edge of the penetrating crack is square-root singular with the regular stress intensity factor $K_I$. It is worth mentioning that the radius of the dominance domain of the square-root singular field is only few microns as detailed numerical calculations revealed. Outside this domain the singular

stress field (3) still prevails. However, the intensity of the singular stress field (3) caused by pure thermal loading, $H_2^{\mathrm{r}}$, is significantly reduced. This is associated with the sharp change of residual stress between ATZ and AMZ layer. To find the reduced GSIF $H_2^r$ associated with the crack increment $\Delta a$ the ERR for a straight crack increment calculated using a simplified version of the expression in Eq. (6) for pure thermal loading was compared with the regular ERR calculated using standard fracture mechanics procedures (for pure thermal stresses) as:

$$W_S^{2\delta_2}\frac{2\delta_2}{2W_S}\left(kH_2^r\right)^2 K_{2p}\left(\varphi_p=0\right)\eta^{2\delta_2-1}=\frac{\left(1-\nu^2\right)}{E_{AMZ}}\left(K_I^r\right)^2, \tag{9}$$

where $\eta=\Delta a/W_S$ and $k$ is a dimensionless coefficient which describes the reduction of GSIF $H_2^{\mathrm{r}}$. The coefficient $k$ can be found from the numerical calculations of $K_{\mathrm{I}}^{\mathrm{r}}$, specifically $k \cong 0.22$. If the reduction of GSIF $H_2^r$ is applied in the crack deflection/branching analysis, a very good agreement with experimental data is obtained. Fig. 6 shows that the crack branches/deflects at the angle $\varphi_{\mathrm{p}} \cong 22°$ for the loading force F ≅220 N when the additional energy $\Delta W$ (see Eq. (4)) is starting to be greater than zero. It can be also inferred from Fig. 6 that crack bifurcation is preferred to crack deflection, because the change of the potential energy $\delta\Pi$ during crack bifurcation is (slightly) greater than that corresponding to single crack deflection. The key feature in the design is the high residual compressive stress in the AMZ layer, which is present in laminate configurations with relative high material volume ratio (i.e. $V_{\mathrm{ATZ}}/V_{\mathrm{AMZ}} \geq 5$). In laminate configurations with lower volume ratios the residual stresses are lower and the inclined single penetration of the crack might be preferred to crack bifurcation.

## 4. Conclusions

A semi-analytical model for the prediction of the crack propagating through the ceramic laminate designed with high compressive residual stresses was presented. A crack bifurcation effect (simultaneous penetration in two directions at a given angle) was discussed and its prediction was compared with experimental observations. The proposed fracture criterion, based on the Finite Fracture Mechanics, can predict both the type and also the angle of the further crack propagation. The crack bifurcation observed in experiments can be explained with the proposed model. The key feature in the design is the high residual compressive stress in the AMZ layer, which is present in laminate configurations with relative low volume ratio between the AMZ and ATZ material (i.e. $t_{\mathrm{AMZ}}/t_{\mathrm{ATZ}} \leq 1/5$). In laminate configurations with higher volume ratios the residual stresses are lower and the inclined single penetration of the crack is preferred to the crack bifurcation.

## References

[1] Bermejo, R., Danzer R. (2010), *Engn. Fract. Mechanics* 77, 2126-2135.
[2] Chen, C.R., Bermejo, R., Kolednik, O. (2010), *Engn. Fract. Mechanics* 77, 2567–2576.
[3] Taylor, D. (2007), *The Theory of Critical Distances.* Elsevier, UK.
[4] Bermejo, R., Torres, Y., Baudin, C., Sánchez-Herencia, A.J., Pascual, J., Anglada, M. et al. (2007) *J Eur Ceram Soc* 27**,** 1443-1448
[5] Kotoul, M., Ševeček, O., Profant, T.: (2010), *Eng. Fract. Mechanics*, 77, 229-248.
[6] Desmorat, R., Leckie, F.A. (1998) *Eur. J. of Mechanics - A/Solids* **17,** 33-52.
[7] Ševeček, O., Kotoul, M., Profant, T. (2012) *Eng Fract Mech* **80,** 28-51.
[8] Martin, E., Leguillon, D., Lacroix, C. (2001) *Composites Sci Technol* **61,** 1671-1679.

The authors gratefully acknowledge a financial support of the Czech Science foundation under the Project No. 101/09/1821.